



On-demand regulation and enhancement of the nucleation in acoustic droplet vaporization using dual-frequency focused ultrasound

Yubo Zhao^a, Dui Qin^b, Junjie Chen^a, Jin Hou^c, Tali Ilovitsh^d, Mingxi Wan^a, Liang Wu^{a,*}, Yi Feng^{a,*}

^a The Key Laboratory of Biomedical Information Engineering of Ministry of Education, Department of Biomedical Engineering, School of Life Science and Technology, Xi'an Jiaotong University, Xi'an, People's Republic of China

^b School of Bioinformatics, Chongqing University of Posts and Telecommunications, Chongqing, People's Republic of China

^c Department of Otorhinolaryngology Head & Neck Surgery, Second Affiliated Hospital of Xi'an Jiaotong University, Xi'an, People's Republic of China

^d Department of Biomedical Engineering, Tel Aviv University, Tel Aviv 6997801, Israel

ARTICLE INFO

Keywords:

Dual-frequency focused ultrasound
ADV nucleation
On-demand regulation
Driving frequency
Acoustic power

ABSTRACT

Acoustic droplet vaporization (ADV) plays an important role in focused ultrasound theranostics. Better understanding of the relationship between the ultrasound parameters and the ADV nucleation could provide an on-demand regulation and enhancement of ADV for improved treatment outcome. In this work, ADV nucleation was performed in a dual-frequency focused ultrasound configuration that consisted of a continuous low-frequency ultrasound and a short high-frequency pulse. The combination was modelled to investigate the effects of the driving frequency and acoustic power on the nucleation rate, efficiency, onset time, and dimensions of the nucleation region. The results showed that the inclusion of short pulsed high-frequency ultrasound significantly increased the nucleation rate with less energy, reduced the nucleation onset time, and changed the length–width ratio of the nucleation region, indicating the dual-frequency ultrasound mode yields an efficient enhancement of the ADV nucleation, compared to a single-frequency ultrasound mode. Furthermore, the acoustic and temperature fields varied independently with the dual-frequency ultrasound parameters. This facilitated the spatial and temporal control over the ADV nucleation, and opens the door to the possibility to realize on-demand regulation of the ADV occurrence in ultrasound theranostics. In addition, the improved energy efficacy that is obtained with the dual-frequency configuration lowered the requirements on hardware system, increasing its flexibility and could facilitate its implementation in practical applications.

1. Introduction

As a powerful protocol for the treatment of cancer and other diseases, high intensity focused ultrasound (HIFU) therapy mainly makes use of thermal effects that are induced by focused ultrasound. In these applications, the deep target tissue needs to reach a high temperature above 65 °C within seconds, resulting in the thermal ablation and coagulative necrosis [1]. Despite being widely employed in for the treatment of tumors including prostate [2], liver [3], breast [4], brain (transcranial) [5] and uterine leiomyomas [6], HIFU still has some inherent limitations including insufficient treatment efficiency, serious side effects, long treatment duration and high equipment requirement due to high energy input [7].

In the clinic, most of the ultrasound therapies approved by Food and

Drug Administration (FDA) use thermal modes of HIFU only [8]. Ultrasound induced cavitation in living tissue is considered unpredictable, due to the unpredictable behavior of bubble nucleation under applied acoustic fields. This constitutes a major drawback in the clinical use of HIFU. However, cavitation is hard to be avoided during HIFU treatment. Thus, the perspective of cavitation in biomedical ultrasound has been shifted in recent years, from inhibiting or monitoring the cavitation to taking advantage of its bioeffects in tissue disintegration [9] or thermal effects enhancement [10,11].

Introducing cavitation nuclei can help to reduce the energy threshold for cavitation and enhance the therapeutic outcome significantly [12]. In recent years, the acoustically sensitive perfluorocarbon (PFC) nanodroplets as small as a few hundreds of nanometers have attractively emerged as an alternative to conventional microbubbles in the enhanced

* Corresponding authors.

E-mail addresses: liangwu@xjtu.edu.cn (L. Wu), fengyi@mail.xjtu.edu.cn (Y. Feng).

<https://doi.org/10.1016/j.ultsonch.2022.106224>

Received 26 August 2022; Received in revised form 29 October 2022; Accepted 3 November 2022

Available online 8 November 2022

1350-4177/© 2022 The Author(s). Published by Elsevier B.V. This is an open access article under the CC BY-NC-ND license (<http://creativecommons.org/licenses/by-nc-nd/4.0/>).

HIFU treatment and ultrasound imaging due to their longer circulation lifetime and smaller size for significant enhanced permeability and retention (EPR) effects *in vivo* relative to microbubbles [13]. PFC nanodroplets could vaporize into microbubbles via ultrasound activation, by phase-shifting from the liquid state to the gas state. This is a physical process termed acoustic droplet vaporization (ADV) [14]. The ADV bubbles have been proved effective in enhancing the acoustic thermal conversion efficiency [15], enhancing inertial cavitation activity [16] and the mechanical bioeffects [17], reducing the acoustic threshold of effective therapy [18], accelerating the ultrasonic heating, shortening the treatment time [19], expanding the injury area and reducing the possibility of complications. Moreover, the excellent ultrasound imaging characteristics of ADV bubble also give PFC nanodroplets a great potential for ultrasound theranostics [20].

Dual- or multiple-frequency ultrasound is also effective to reduce the cavitation threshold or increase cavitation effects compared with standard single-frequency ultrasound. Dual-frequency excitation was utilized for cavitation-enhanced thermal ablation [21], thrombolysis [22–24], and sonodynamic therapy [25], and was able to reduce the inertial cavitation threshold and improve therapeutic efficiency significantly. Numerical studies suggested the potential mechanisms for enhanced bubble cavitation by dual-frequency excitation, which include the unique nonlinear features of superharmonic focusing [26], bubble oscillations [27], the enhancement of the bubble expansion ratio and collapse strength [28], the reduction of inertial cavitation threshold [29], the increase mass transfer through the bubble interface [30] and the alteration of the bubble spherical stability [31]. However, these studies focused on the use of microbubbles rather than PFC nanodroplets.

In our previous studies, dual-frequency HIFU has been introduced with PFC nanodroplets and nanoparticles to increase the efficiency of focused ultrasound therapy in experiments. The combined dual-frequency focused ultrasound pulse consisted of a long pulse at a center frequency of 1.1 MHz and a short pulse at a frequency of 5 MHz. This was shown to reduce the ADV threshold, manipulate the ADV volume and increase the cavitation efficacy [32]. The dual-frequency HIFU was also shown to effectively activate the phase transition of perfluoropentane (PFP) nanoparticles into microbubbles, while significantly reducing the HIFU threshold for thermal ablation lesion in phantoms, enhancing the antitumor efficacy, and realizing ultrasound monitoring imaging *in vitro* and *in vivo* [33]. It indicated a short pulsed high-frequency ultrasound was the main source for ADV, and the long pulsed low-frequency ultrasound increased cavitation-induced bio-effects. Therefore, a dual-frequency ultrasound configuration could act as a potential strategy for higher efficiency at a reduced acoustic power. However, current experimental studies only investigate effects of the acoustic power on ADV process under a specific pair of ultrasound frequencies (i.e. 1.1 MHz and 5 MHz), which could not give a comprehensive understanding of the relationship between the ultrasound parameters and the ADV effects. In particular, how to control the thermal or cavitation effect through regulating the driving frequency and acoustic power of the dual-frequency HIFU is not clear yet.

During ADV, the internal gas nucleation is the initial stage of the formation of the initial vapor bubble nucleus. This determines the subsequent ADV bubble distribution, dynamics and the HIFU treatment efficacy enhancement [34]. To regulate the cavitation effects of PFC nanodroplets on-demand in ultrasound excitation, the internal gas nucleation of ADV (i.e., ADV nucleation) is a crucial process. If the ADV nucleation, which is closely determined by the acoustic pressure and temperature, could be precisely controlled, it would play an important role in an on-demand therapy, aimed at optimized therapeutic outcome while operating at a relatively safe energy range. Compared to single-frequency ultrasound insonation, where the acoustic pressure and the temperature change synchronously with the alternation of ultrasonic parameters, the dual-frequency ultrasound excitation could achieve precise control of ADV nucleation by regulating the temperature and

acoustic fields independently.

Numerical simulations of ADV nucleation in the dual-frequency focused ultrasound could predict the effect of different ultrasound parameters and yield an optimal parameter choice for the regulation of ADV nucleation in the on-demand theranostic applications, e.g. the enhanced HIFU thermal ablation, histotripsy or boiling histotripsy, sonoporation therapy or blood-brain-barrier opening. As a commonly used theory of nucleation, the classical nucleation theory (CNT) has been previously used to study cavitation in biological fluids and tissues [10] as well as nucleation of a bubble in nano- and micro-sized [35] PFP emulsions. It was also proved to be suitable for simulating HIFU cavitation by reasonably and effectively correcting the surface tension of liquid [36]. Here, CNT strongly depend on macroscopic information like temperature and pressure which could be accessible from the acoustic and thermal simulations of the dual-frequency approach.

In this work, a modified CNT was used to simulate the ADV nucleation of PFP nanodroplets activated by a confocal dual-frequency HIFU. The pressure and temperature fields were modelled by the linear Helmholtz and Pennes' Bioheat Transfer equations, respectively. A parametric study was conducted to show the patterns of ADV nucleation rate, efficiency, onset time, and dimensions of the nucleation region under different dual-frequency focused ultrasound conditions. Finally, the effects of the driving frequency and acoustic power on ADV nucleation were analyzed and discussed to give a primary instruction for on-demand regulation of ADV in the dual-frequency focused ultrasound for theranostics.

2. Theory and methods

2.1. Dual-frequency focused ultrasound model

Fig. 1 illustrates the dual-frequency focused ultrasound system used for the PFP nanodroplets ADV nucleation simulation. The ultrasound transducer consisted of two confocal spherical annular elements, which had a similar geometry as used in previous experimental studies [32,33]. The inner ring had a radius r_1 (25 mm) and was stimulated at a high frequency, while the outer ring had a radius r_2 (47 mm) and was stimulated at a lower frequency. The radius r_0 of the central hole and the focal length R_{FU} of the transducer were 11 mm and 60 mm, respectively.

To study the ADV nucleation, the PFP nanodroplets were assumed to be evenly distributed in a tissue phantom with a volume fraction of 10^{-4} .

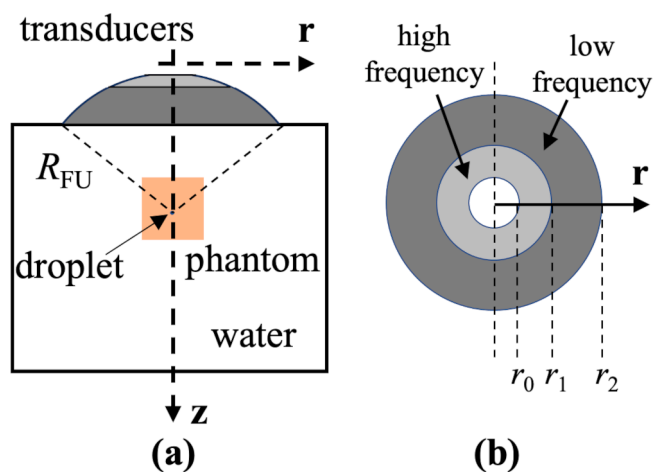


Fig. 1. Schematic diagram of dual-frequency focused ultrasound model. (a) The dual-frequency transducer (dark-gray outer ring for the low-frequency ultrasound and light-gray inner ring for the high-frequency ultrasound) and the tissue phantom (orange solid square) filled with PFP nanodroplets. The R_{FU} is the focal distance of the transducer. (b) The shape of the dual-frequency transducer in the axial view. The r_0 , r_1 , and r_2 represent the radius of the central hole, inner ring, and outer ring, respectively.

The phantom was a cylinder with a radius of 50 mm and a length of 60 mm, and located at the focal point and coaxial with the transducer. In addition, both the transducer and the phantom were immersed in water. It should be pointed out that the tissue-mimicking phantom used in the simulation was chosen based on its simple geometry and acoustic propagation, which can be easily reproduced experimentally. In this model, the phantom did not refer to a specific type of human tissue, but was set as a uniform medium with average values of physical properties for human soft tissue, e.g. density $\rho = 1044 \text{ kg/m}^3$ and speed sound $c = 1568 \text{ m/s}$ [37].

The acoustic field generated by the dual-frequency ultrasound was solved using the linear Helmholtz equation in two dimensional axisymmetric cylindrical coordinates [38]:

$$\frac{\partial}{\partial r} \left[-\frac{r}{\rho} \left(\frac{\partial p}{\partial r} \right) \right] + r \frac{\partial}{\partial z} \left[-\frac{1}{\rho} \left(\frac{\partial p}{\partial z} \right) \right] - \left[\left(\frac{\omega}{c} \right)^2 \right] \frac{rp}{\rho} = 0, \quad (1)$$

where r and z are radial and axial coordinates, p is the pressure output from the focused transducer, and $\omega = 2\pi f$ is the angular frequency, in which f is the driving frequency of the ultrasound. Based on the assumption that the transducer vibration and particle vibration on the transducer surface were continuous and consistent, the acoustic pressure p on the transducer surface had a linear relationship with the transducer vibration d , i.e. $p = \omega\rho c \cdot d$. For simplification, the acoustic wave propagation was assumed to be linear and nonlinear effect was neglected. Because linear acoustic is valid when $p \ll \rho c^2$ [39], and the maximal pressure (22.5 MPa) in all simulation conditions was much smaller than the product $\rho c^2 = 2567 \text{ MPa}$, the assumption of linear wave propagation in this study was reasonable.

For heat generation induced by the dual-frequency focused ultrasound, the temperature T in the tissue phantom was calculated by the Pennes' Bioheat Transfer equation:

$$\rho C_p \frac{\partial T}{\partial t} = \nabla \cdot (k \nabla T) + Q, \quad (2)$$

where Q is the heat source due to the absorbed ultrasound energy determined by $Q = 2\alpha I$, in which I is the acoustic intensity obtained from the acoustic field, i.e. $I = \frac{p^2}{2\rho c}$. In this simulation, the initial temperature of the PFP nanodroplets in the phantom was 298.15 K (i.e. 25 °C), while the specific heat C_p , thermal conductivity k , and acoustic absorption coefficient α were 3710 J/(kg·K), 0.59 W/(m·K), and 8.55 Np/m/MHz, respectively [38].

2.2. ADV nucleation model for a PFP nanodroplet

A modified classical nucleation theory, as proposed in previous studies [40,41], was used to simulate the ADV nucleation process of a PFP nanodroplet in the dual-frequency ultrasound. At a specific pressure p_l and temperature T_l , the critical radius r^* and work W^* for nucleation was calculated by

$$r^*(T_l, p_l) = \frac{2\sigma_r(T_l, p_l)}{p_v - p_l}, \quad (3)$$

$$W^*(T_l, p_l) = \frac{16\pi\sigma_r^3(T_l, p_l)}{3(p_v - p_l)^2}, \quad (4)$$

where σ_r is the size-dependent surface tension by considering the effect of the nucleus curvature based on a scaling function [41,42], i.e.

$$\sigma_r(T_l, p_l) = \sigma_\infty(T_l) \sqrt[3]{(1 - \xi)(1 + 0.5\xi)^2}, \quad (5)$$

$$\xi = \frac{p_v(T_l) - p_l(T_l)}{p_v(T_l) - p_{spin}(T_l)}, \quad (6)$$

where $\sigma_\infty(T_l) = 0.0425 \left(1 - \frac{T_l}{T_c}\right)^{1.2}$ is the temperature-dependent surface tension of flat interface [43], and ξ is a normalized degree of liquid metastability determined by the local pressure p_l in the PFP nanodroplet, the vapor pressure p_v in the nucleus, and spinodal pressure p_{spin} of the metastable phase, which are given by

$$p_l = p_\infty + p_{lap} + p_a \quad (7)$$

$$p_v(T_l, p_l) = p_{sat}(T_l) \cdot \exp\left(-\frac{p_{sat}(T_l) - p_l}{\rho_l R T_l}\right), \quad (8)$$

where p_∞ , p_{lap} , p_a , and p_{sat} are the ambient pressure (1 atm), Laplace pressure, applied acoustic pressure, and saturation vapor pressure, respectively. The modifications given by Eqs. (5) and (6) take into account the deviation of the surface tension for the nano-sized critical nucleus σ_r from the bulk value σ_∞ , yielding a vanishing work of nucleation at the spinodal points [41,42]. In the simulation, the acoustic pressure p_a was the solution of the dual-frequency acoustic field from Eq. (1), while the Laplace pressure $p_{lap} = 2\sigma_d/R_d$ was related to the surface tension at the PFP nanodroplet surface $\sigma_d = 56 \text{ mN/m}$ and its size $R_d = 100 \text{ nm}$ of the PFP nanodroplet. For more details of the nucleation model, please refer to [40,41].

2.3. Simulation conditions and data analysis

A parametric study was conducted to investigate the effects of dual-frequency ultrasound on the ADV nucleation. During the simulation, a continuous low-frequency ultrasound and a pulsed high-frequency ultrasound with 1 % duty cycle were applied to generate the dual-frequency acoustic field and thermal field. For the low-frequency ultrasound, three different driving frequencies (LF = 0.5, 1.0, and 1.5 MHz) [44] and eleven different acoustic powers (LW from 0 to 50 W with a step of 5 W) were selected as used in normal single-frequency focused ultrasound. For the high-frequency ultrasound, a wide range of driving frequencies (HF = 2, 3, 4, and 5 MHz) and acoustic powers (HW from 0 to 10 W with a step of 1 W) were studied to evaluate its contributions to the ADV nucleation in the dual-frequency focused ultrasound [45]. In this model, the acoustic power W was implemented using the vibration amplitude of the transducer d , i.e. $d = \frac{1}{2\pi f} \sqrt{\frac{2W}{\rho c S}}$, in which f is the driving frequency and S is the area of the transducer surface. The vibration amplitudes applied in the simulation under different acoustic power were shown in the Fig. S1 in the supplementary information. For each condition, the pulse-repetition frequency and irradiation time of the focused ultrasound were 100 Hz and 5 s.

In this study, a total of 1270 conditions were simulated to analyze the varying patterns in their rate, onset time, and spatial profiles of the ADV nucleation under different combinations of the dual-frequency focused ultrasound parameters. As in previous studies [10,41], the nucleation rate was defined as the number of critical nuclei formed per unit time and volume, given in a logarithmic form by

$$\lg J(T_l, p_l) = \log_{10} \left(\sqrt{\frac{3\sigma_r(T_l, p_l)\rho_l^2}{\pi m^3}} \cdot \exp\left(-\frac{W^*(T_l, p_l)}{k_B T_l}\right) \right), \quad (9)$$

where ρ_l is the PFP liquid density, m is the mass of single molecule, and k_B is the Boltzmann constant. Accordingly, a nucleation efficiency E_J was quantified as the ratio of the nucleation rate to the total acoustic power of the dual-frequency focused ultrasound, i.e.

$$E_J = \frac{\lg J}{LW + HW}, \quad (10)$$

given in units of nuclei per watt. The E_J measures the ability to produce the ADV nucleus per unit of acoustic power under a specific dual-frequency condition. Generally, a higher value of E_J indicates a higher efficiency of energy utilization during ADV nucleation process.

Furthermore, to investigate the onset time and spatial dimensions of the ADV nucleation, the number of the critical nuclei formed in a volume V_0 within a time interval τ_0 was approximated in a logarithmic form by

$$\lg N_J = \log_{10}(JV_0\tau_0), \quad (11)$$

where $V_0 = 1 \times 10^{-6} \text{ mm}^3$ is the spatial resolution selected in the simulation and $\tau_0 = 1/(10f)$ is a period during which the lowest pressure and constant temperature are guaranteed, where f is the driving frequency of the high-frequency ultrasound in the dual-frequency ultrasound conditions [10,11].

As a result, a nucleation onset time t_J was defined as the minimal irradiation time needed to form the first critical nuclei (i.e. $\lg N_J = 0$) in the focal volume, while the nucleation site was recognized as the area where at least one critical nuclei was formed (i.e. $\lg N_J \geq 0$) and evaluated by measuring the length a , width b , length-width ratio a/b , and volume V of the nucleation region. Because the nucleation region was approximately an ellipsoid, the a and b were the major and minor axes of the ellipsoid respectively, while the V was defined by the ellipsoid volume formula, i.e. $\pi ab^2/6$.

3. Results and discussion

3.1. Acoustic field and temperature distribution

Fig. 2 compares the peak negative pressure magnitude under the single- and dual-frequency ultrasound conditions. As expected, an oval-like distribution of the negative pressure was observed in either single or dual-frequency ultrasound acoustic field. For the single-frequency ultrasound cases [Fig. 2(a) and (b)], a higher driving frequency produced more focused acoustic field with a smaller length and width of the elliptic focus [44]. In addition, although the acoustic power of the high-frequency ultrasound was much lower than that of the low-frequency ultrasound, the negative pressure magnitudes in these two acoustic fields were comparable, indicating that the high-frequency ultrasound can make a great contribution to the acoustic field. As shown in Fig. 2(c), the dual-frequency ultrasound generated a much higher negative pressure than the single-frequency ultrasound, which can also be seen from the focal waveforms shown in Fig. S2 in the supplementary information and is better for the ADV nucleation [46]. Also, the peak negative pressure under different dual-frequency ultrasound conditions was compared as shown in Fig. 2(d). The results indicate a significant and

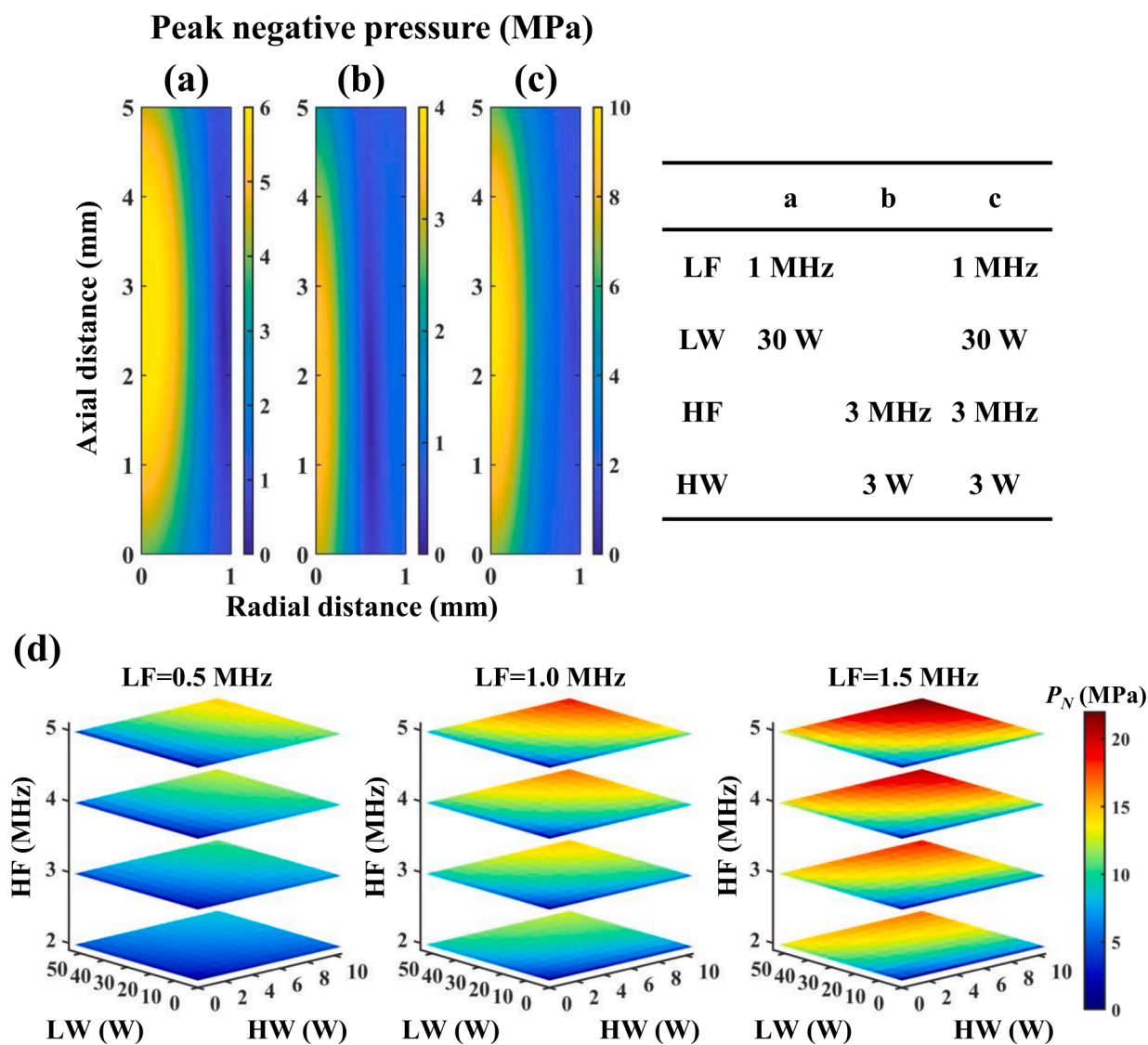


Fig. 2. Peak negative pressure distribution in the acoustic field of the (a) low-frequency ultrasound with LF = 1 MHz and LW = 30 W, (b) high-frequency ultrasound with HF = 3 MHz and HW = 3 W, and (c) dual-frequency ultrasound under the conditions of (a) and (b). (d) Peak negative pressure under different dual-frequency focused ultrasound conditions.

positive correlation between the peak negative pressure and any ultrasound parameter, and there is little difference in the contribution of the low-frequency and high-frequency ultrasound to the acoustic field. However, it should be noted that the acoustic power of the high-frequency ultrasound was much lower than that of the low-frequency ultrasound, meaning a greater impact of the high-frequency ultrasound on the acoustic field.

For the dual-frequency ultrasound system, since the high-frequency ultrasound was working in a pulse mode with a very small duty cycle, its impact on the temperature was slight during limited irradiation [47], as shown in Fig. 3. As a result, the temperature changes over time and space were determined by the low-frequency ultrasound. Firstly, the temperature gradually increased with irradiation time, and the increase rate was positively related with the driving frequency and acoustic power. Secondly, temperature distribution in space had a similar shape as the acoustic field of the low-frequency ultrasound [see Fig. 2(a)]. Also, the isothermal lines qualitatively showed an uneven increase of the temperature around the focus, i.e. a faster temperature rise in the radial direction than the axial direction. Because the temperature is an important factor that affects the ADV nucleation as shown in Eqs. (4) and (9), the higher the driving frequency and acoustic power of the low-frequency ultrasound, the larger the temperature increase at the acoustic focus area and consequently the greater the thermal effect on the ADV nucleation in the dual-frequency ultrasound system.

3.2. Nucleation rates and efficiency

Fig. 4 shows the effects of driving frequency and acoustic power on the nucleation rates in the dual-frequency focused ultrasound. In general, as the driving frequency and acoustic power of either the low- or high-frequency ultrasound increased, the nucleation rate went up as well, indicating a positive relationship between the nucleation occurrence and dual-frequency ultrasound parameters. During the ADV nucleation, the nucleation rates increased with the liquid temperature and/or the pressure increasing [see Fig. S3 in the supplementary information], as the acoustic power of the low- or high-frequency ultrasound increased. These variation tendencies are consistent with those of the nucleation rate for water in histotripsy under the single-frequency focused ultrasound excitation [10,11,48]. Nevertheless, it should be noted that the nucleation thresholds in ADV and histotripsy are greatly different, specifically the latter usually requires a larger threshold. It can be explained due to the discrepancies between the thermodynamic properties of the metastable PFP and water where nucleation occurs [49–52]. Moreover, by comparison, the nucleation rate had a larger variation as increasing the low-frequency parameters than the high-frequency parameters, especially in the conditions with a low-frequency ultrasound whose driving frequency was relatively large (i.e. 1.5 MHz). This difference in effects is resulted from the short duty cycle (1 %) and small acoustic power (≤ 10 W) of the pulsed high-frequency ultrasound, indicating a leading role of the low-frequency ultrasound in the dual-frequency system.

Nonetheless, the high-frequency ultrasound parameters still had a

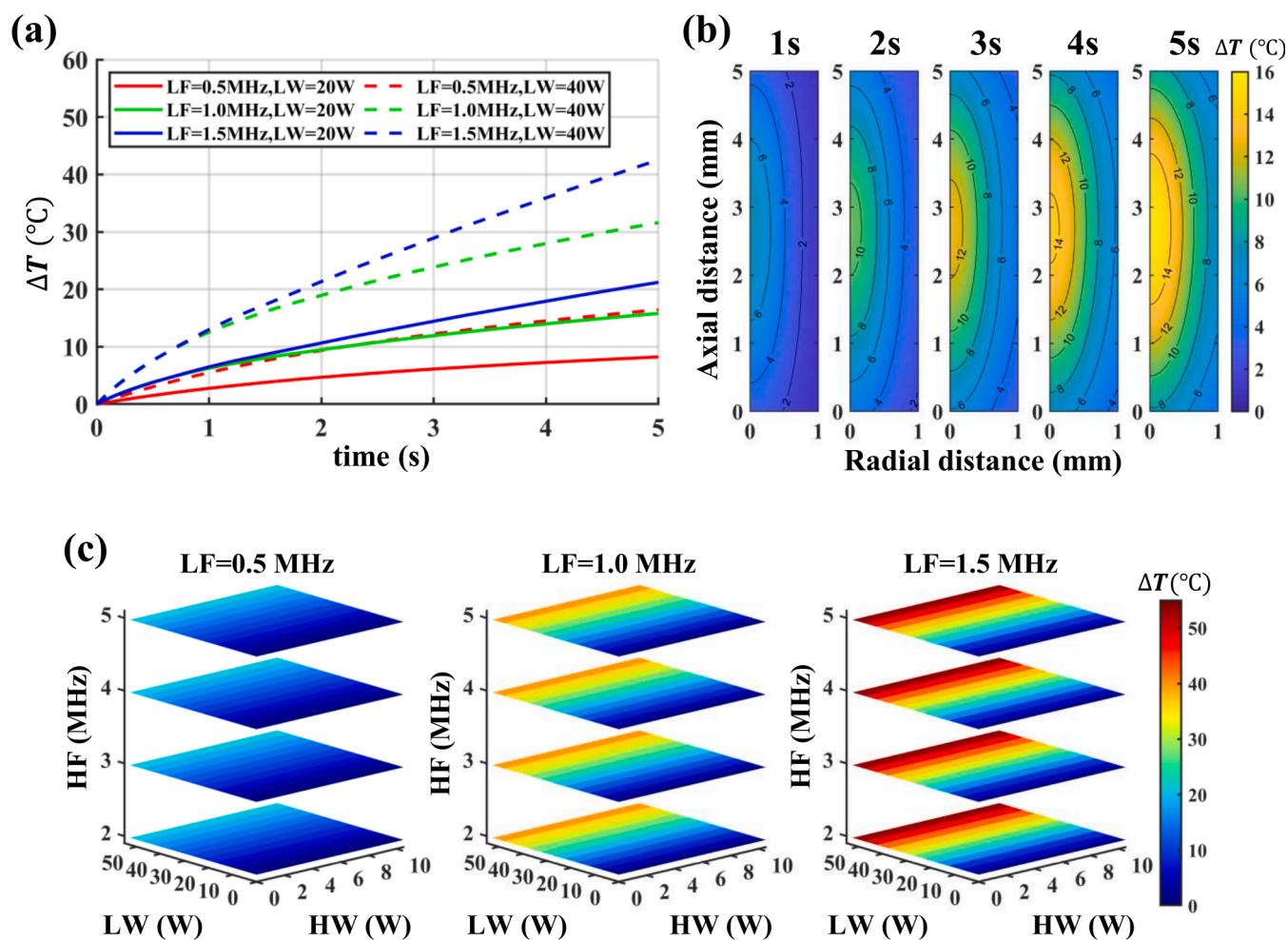


Fig. 3. Time-dependent temperature variation (a) at the focus under different focused ultrasound conditions and (b) around the focal region under the condition with LF = 1 MHz, LW = 20 W. (c) Temperature rise under different dual-frequency focused ultrasound conditions after 5 s irradiation.

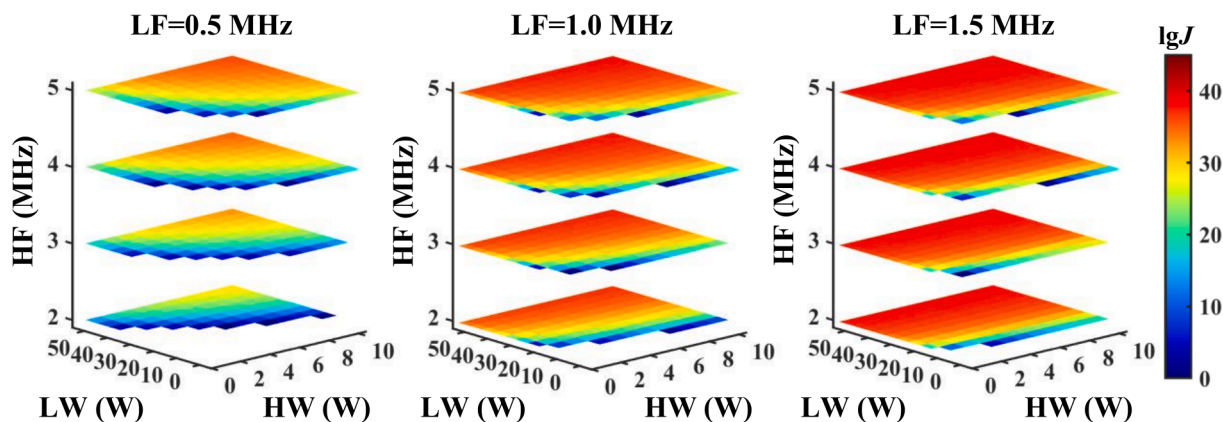


Fig. 4. Nucleation rates under different dual-frequency focused ultrasound conditions after 5 s irradiation. Cases with $HW = 0$ are equivalent to the normal single-frequency focused ultrasound conditions. Regions without data indicate conditions of no nucleation.

significant impact on the nucleation rate, particularly in the cases where the driving frequency of the low-frequency ultrasound was small (e.g. 0.5 MHz). When the low-frequency ultrasound parameters were kept constant, inclusion of the high-frequency ultrasound was able to cause a noticeable increase in the nucleation rate, and could even make nucleation possible in some conditions where the nucleation cannot be activated by the single-frequency ultrasound (i.e. $HW = 0$). This outcome implies that the dual-frequency ultrasound is easier to generate ADV nucleation than the single-frequency ultrasound [53].

From the aspect of energy supply, inclusion of the high-frequency ultrasound reduced the minimal acoustic power of the low-frequency ultrasound required for the nucleation activation. For example, the nucleation acoustic power threshold at 1-MHz single-frequency ultrasound condition was 20 W, which dropped to 15 W just by applying a 2-MHz high-frequency ultrasound at a small acoustic power (1 W). This result is mainly because, at the same acoustic power, the focused ultrasound with a higher driving frequency has a greater contribution to the negative pressure [54]. Consequently, the lower the driving frequency of the low-frequency ultrasound, the stronger the effect of the high-frequency ultrasound, e.g. a 5-W 3-MHz high-frequency ultrasound could reduce the acoustic power by >40 W for 0.5-MHz low-frequency ultrasound but <10 W for 1.5-MHz low-frequency ultrasound.

Furthermore, the dual-frequency ultrasound can achieve a specific nucleation rate with a less total acoustic power than the single low-frequency ultrasound. For example, the total acoustic power for nucleation activation was 20 W using a 1-MHz single-frequency ultrasound but only 7 W using a 1-MHz (5 W) and 5-MHz (2 W) dual-frequency ultrasound system. This result indicates that energy dissipation in the

single-frequency ultrasound is high, and the dual-frequency ultrasound is able to lower energy consumption and improve nucleation efficiency.

Fig. 5 shows the quantitative evaluation of the nucleation efficacy under different dual-frequency focused ultrasound conditions. In similarity to the nucleation rate, the nucleation efficiency generally increased as increasing the driving frequency of either low-frequency or high-frequency ultrasound. However, as the acoustic power changed, the nucleation efficiency E_J showed visible differences in variation patterns from the nucleation rate. Above all, the nucleation efficiency significantly decreased with the increase of the acoustic power of the low-frequency ultrasound. This trend indicates that although increasing acoustic power of the low-frequency ultrasound can increase nucleation rate [see Fig. 4], the reduced nucleation efficiency implies more energy wasted in the nucleation process, which may be related to the energy absorption in the tissue [see Fig. 3]. By contrast, high-frequency pulsed ultrasound had little thermal effect, increasing acoustic power of the high-frequency ultrasound contributed more energy to the acoustic pressure [see Fig. 2], which could increase the nucleation rate and avoid energy dissipation, thus improving the nucleation efficiency. However, the nucleation efficiency didn't monotonically increase with the acoustic power of the high-frequency ultrasound and had a peak value, e.g. the maximal E_J occurred at $HW = 7 \sim 8$ W for the conditions with ($LF = 0.5$ MHz, $HF = 5$ MHz), while appeared at $HW = 2 \sim 4$ W for the conditions with ($LF = 1.5$ MHz, $HF = 5$ MHz). This result can be explained by the fact that the nucleation rate obtained by the CNT model is gradually approaching a limit value (i.e. $\lg J \approx 38$) as increasing acoustic power of the high-frequency ultrasound [10, 11, Fig. S3 in the supplementary information]. Accordingly, a decreased E_J is expected to

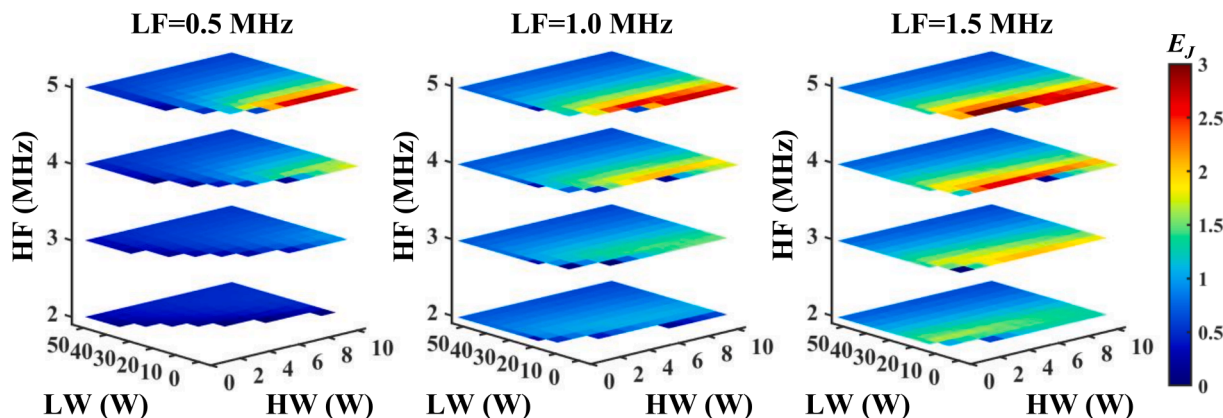


Fig. 5. Nucleation efficiencies under different dual-frequency focused ultrasound conditions after 5 s irradiation. Cases with $HW = 0$ are equivalent to the normal single-frequency focused ultrasound conditions. Regions without data indicate conditions of no nucleation.

happen when the increase of the nucleation rate is slower than the total acoustic power as defined by Eq. (10). Furthermore, for a specific system condition (i.e. HF and LF), there is always an optimal pair of ultrasound parameters (i.e. HW and LW) to produce a maximal nucleation efficiency. Therefore, reducing acoustic power of the low-frequency ultrasound and selecting an optimal acoustic power of the high-frequency ultrasound are beneficial to improving energy utilization and increasing nucleation efficiency [29].

In addition, the low-frequency continuous ultrasound mainly determines the temperature field [see Fig. 3], and accordingly a low acoustic power of the low-frequency ultrasound leads to a small temperature increase within the tissue, which is important for the safety and sometimes necessary in the therapy using heat-labile drugs or SDT reagents [10,11,48]. With the same nucleation efficiency, the required acoustic power of the low-frequency ultrasound can be distinctly reduced as the driving frequency and acoustic power of the high-frequency ultrasound increase in the dual-frequency ultrasound cases. From another perspective, high nucleation efficiency means that more energy from the power supply is used to induce ADV nucleation. Therefore, the fact that dual-frequency ultrasound can reduce the acoustic power of the low-frequency ultrasound shows a potential advantage of the dual-frequency ultrasound in temperature and safety control, and the metric of nucleation efficiency E_J may be a potential parameter for the dosimetry of protocols and optimization of energy consumption in the future system design.

3.3. Nucleation onset time

Fig. 6 shows the onset time of the nucleation at the focus under different dual-frequency focused ultrasound conditions. Firstly, similar as in the single-frequency focused ultrasound [10,11,48], the nucleation onset time in the dual-frequency system decreased monotonically with increasing the driving frequency and acoustic power of the low-frequency ultrasound due to higher pressure and faster temperature rise. Secondly, inclusion of the high-frequency ultrasound also significantly shortened the irradiation time for nucleation, and this effect was enhanced with increasing the driving frequency or acoustic power of the high-frequency ultrasound. For example, the nucleation onset time at the condition with LF = 1 MHz and LW = 35 W was 4.45 s, which could be reduced to 2.16 s by adding a 1-W 2-MHz ultrasound or to 0.95 s by using a 1-W 4-MHz ultrasound. This outcome is mainly because the contribution of the high-frequency ultrasound to the pressure field compensates the thermal effect required for nucleation, thus reducing the time of the temperature rise, i.e. irradiation time of the low-frequency ultrasound.

Furthermore, the nucleation onset time in many conditions were shown to be zeros, indicating extreme conditions that the nucleation can

be activated in a very short timescale after the ultrasound irradiation. This is mostly due to the higher acoustic pressure than the nucleation pressure threshold (8.2 MPa) at the initial temperature (25 °C), which means that the nucleation can be caused exclusively by the ultrasound tensile pressure. In theory, this case can also be achieved in the single-frequency ultrasound with a high enough acoustic power, e.g. > 50 W at the condition with LF = 1 MHz, but by contrast, the dual-frequency system significantly reduces the total acoustic power, e.g. 20 W (LF = 1 MHz) + 5 W (HF = 4 MHz). On the one hand, this result again demonstrates a high energy efficiency for the dual-frequency ultrasound system. On the other hand, the thermal effect can be greatly weakened in the dual-frequency system, even for applications requiring long-time irradiation.

Similar nucleation onset times (e.g., approximately 2 s) were observed in different conditions, e.g. (LF = 1 MHz, LW = 45 W), (LF = 1 MHz, LW = 30 W, HF = 2 MHz, HW = 3 W), (LF = 1 MHz, LW = 15 W, HF = 4 MHz, HW = 4 W), and (LF = 0.5 MHz, LW = 45 W, HF = 4 MHz, HW = 4 W). These results indicate that the dual-frequency ultrasound has multiple combinations that are able to achieve the same nucleation onset through complementary effects between different ultrasound parameters. This provides a better flexibility for the dual-frequency ultrasound method for therapeutic applications that have different needs and equipment constraints.

3.4. Spatial-temporal variation of nucleation region

The spatial variations of the nucleation site over irradiation time under single- and dual-frequency focused ultrasound are illustrated in Fig. 7. From the spatial point of view, both the single- and dual-frequency ultrasound generated an elliptical nucleation area with a major axis along the axial direction, which is similar as the shape of the acoustic field shown in Fig. 2. Then, as the irradiation time increased, the nucleation site grew gradually in all directions, and the variation trend of the nucleation site with time was consistent in different ultrasound conditions. Qualitatively, the only difference of the nucleation site between the single- and dual-frequency ultrasound was that the inclusion of the high-frequency ultrasound greatly increased the dimensional size of the nucleation region, which might be attributed to the effect of the dual-frequency ultrasound on the nucleation rate [discussed in Section 3.2].

From the temporal perspective, typical trends of the nucleation region change in the length, width, length–width ratio, and volume are illustrated in Fig. 8. Except the ones without nucleation, the nucleation site of all conditions had increased length and width as the irradiation time increased, thus leading to an increased nucleation volume over time. But the rate of increase in the volume gradually decreased, which is similar as the trend of temperature change [see Fig. 3(a)], indicating

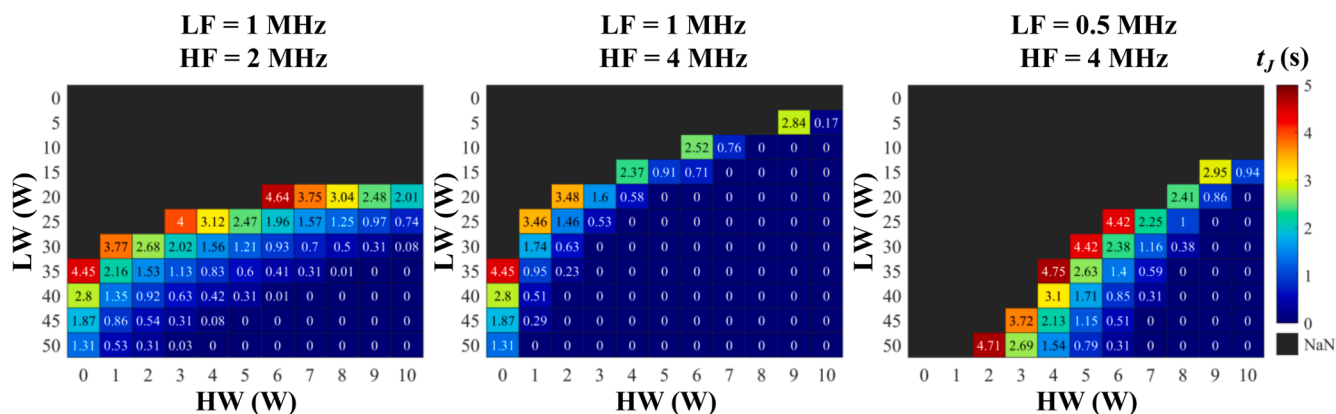


Fig. 6. Minimal irradiation time needed to generate nucleation under different dual-frequency focused ultrasound conditions. The zero value indicates immediate occurrence of nucleation after the irradiation, while region without data indicate no nucleation occurred within 5 s irradiation.

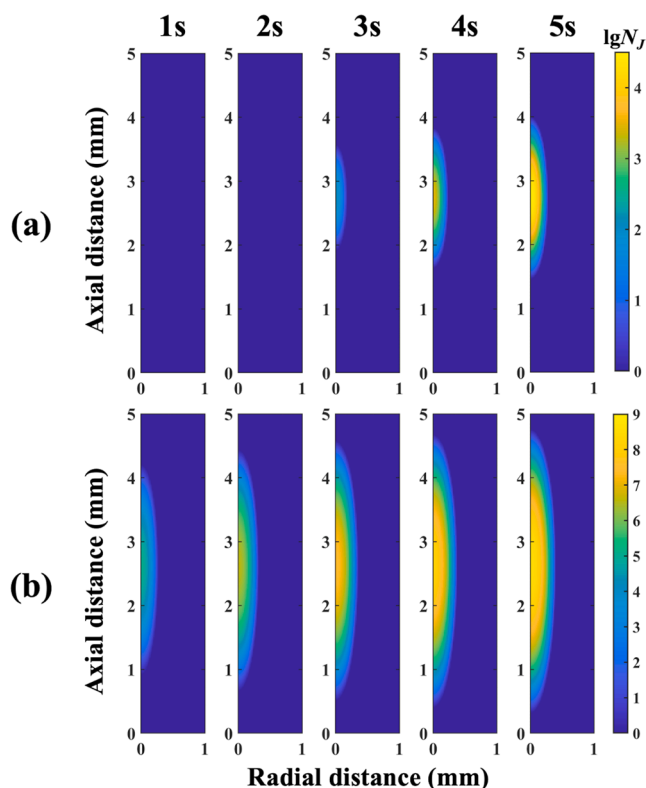


Fig. 7. Typical time-dependent spatial distribution of the nucleation occurrences under (a) single-frequency and (b) dual-frequency focused ultrasound conditions. In this case, the parameters of the single-frequency ultrasound are LF = 1 MHz and LW = 30 W, while the parameters of the dual-frequency ultrasound are LF = 1 MHz, LW = 30 W, HF = 3 MHz, and HW = 3 W.

that expansion of the nucleation region is mainly determined by the thermal effect, i.e. the low-frequency ultrasound. In addition, another evidence showing the importance of the thermal effect was a progressive decrease in the length–width ratio, which means a faster increase in the width than the length. This difference of the increase rates in different directions is consistent with the temperature changes in space as shown in Fig. 3(b).

Fig. 8 also shows the dimensional differences of the nucleation site over time between single- and dual-frequency focused ultrasound. Firstly, the inclusion of the high-frequency ultrasound significantly increased the length, width, and volume of the nucleation site, which is due to the increased nucleation rates under the dual-frequency ultrasound conditions. Secondly, the differences between the length–width ratio curves under different LW conditions were magnified in the dual-frequency ultrasound, indicating significant but different effects of the high-frequency ultrasound on the length and width and possibility of controlling the shape of nucleation site. But even so, there is no significant change in the variation patterns of each measure.

In order to quantitatively evaluate the effect of the dual-frequency ultrasound parameters on the nucleation site, the length, width, length–width ratio, and volume of the nucleation region after 5 s irradiation under different conditions are shown in Fig. 9. For the length and width of the nucleation site, they increased with increasing acoustic power of either low- or high-frequency ultrasound. However, the effect of the HW on the width was much weaker than on the length, due to the fact that the expansion of the nucleation region in the radial direction is largely dependent on the thermal effect, i.e. the low-frequency ultrasound.

Regarding the driving frequency, the LF had a larger impact on the length and width than the HF, while the HF showed a greater effect in the conditions with lower LF (e.g. 0.5 MHz), which is similar as the

effects on the nucleation rate due to the short duty cycle of the high-frequency ultrasound. But unlike the variation patterns of the nucleation rate, the length and width didn't vary monotonically with the LF but had peak values at the conditions with LF = 1.0 MHz. This outcome could be explained by the following two aspects of the LF effects: 1) The higher LF generates a more focused acoustic field [see Fig. 2], thus leading to a smaller length and width; 2) The higher LF produces a rapid rise and expansion of the temperature field, thus resulting in a larger dimensional size of the nucleation region, especially the width. Consequently, the contrary effects of the LF codetermines an increasing–decreasing pattern of the length and width variation, especially in high LW conditions.

Since the length–width ratio and volume were defined by the length and width, the effects of the parameters on the length–width ratio and volume were highly related to the effects on the length and width. For the length–width ratio, it had a negatively relationship with the low-frequency ultrasound parameters but was positively correlated with the high-frequency ultrasound parameters. This is because the thermal effect controlled by the low-frequency ultrasound has a larger effect on the width than the length. When the effect of the low-frequency ultrasound was small at low LF or LW, the effect of the HF and HW became noticeably stronger. For the volume of the nucleation site, because it was proportional to the square of the width, the volume had a closer variation pattern to the width.

3.5. The regulation of ADV nucleation in the dual-frequency focused ultrasound

The goal of this work was to understand the physical mechanism of dual-frequency focused ultrasound ADV nucleation through the assessment of the ultrasound parameters effects (i.e. driving frequency and acoustic power) on the nucleation rate and efficiency, onset time, and nucleation region volume. Overall, all the parameters of the dual-frequency ultrasound affect the nucleation by changing the acoustic field and the temperature field, as was shown previously with single-frequency ultrasound [10,11,48]. However, in the dual-frequency ultrasound system using in this study, the continuous low-frequency ultrasound affects both the pressure distribution and temperature variation, while the pulsed high-frequency ultrasound mainly influences the acoustic field. This gives the dual-frequency ultrasound a major advantage of an independent control over the acoustic pressure and temperature, which is not feasible using the single-frequency ultrasound [10,11,48]. In practice, this advantage could bring a benefit of optimal temperature and nucleation control. For example, the dual-frequency ultrasound could be beneficial for applications that require low temperature and high nucleation, using a low-power continuous ultrasound to control the temperature rise and utilizing a pulsed high driving frequency ultrasound to regulate the nucleation rate and region.

Another key advantage of the dual-frequency ultrasound is that the total input power can be greatly reduced, which is primarily due to significant increase in the nucleation rate after adding the high-frequency ultrasound. The basic rationale behind this result is that high-frequency ultrasound provides higher negative pressure than the low-frequency ultrasound under the same input power condition, showing a best use of the characteristics of the high-frequency ultrasound. In practical application, the benefit of this advantage is high energy utilization and low energy supply, further lowering the requirements on the system.

Furthermore, it is worth noting that the effects of each ultrasound parameter on the different nucleation measures, i.e. efficiency, onset time, and dimensions, are different or even opposite. For instance, a lower LW and higher HF causes a higher nucleation efficiency [see Fig. 5] but a smaller cigar-shaped nucleation region [see Fig. 9]. As a result, a trade-off between different measures, like the nucleation efficiency and the volume of nucleation site, should be considered and controlled through regulating different parameters. Fortunately, the

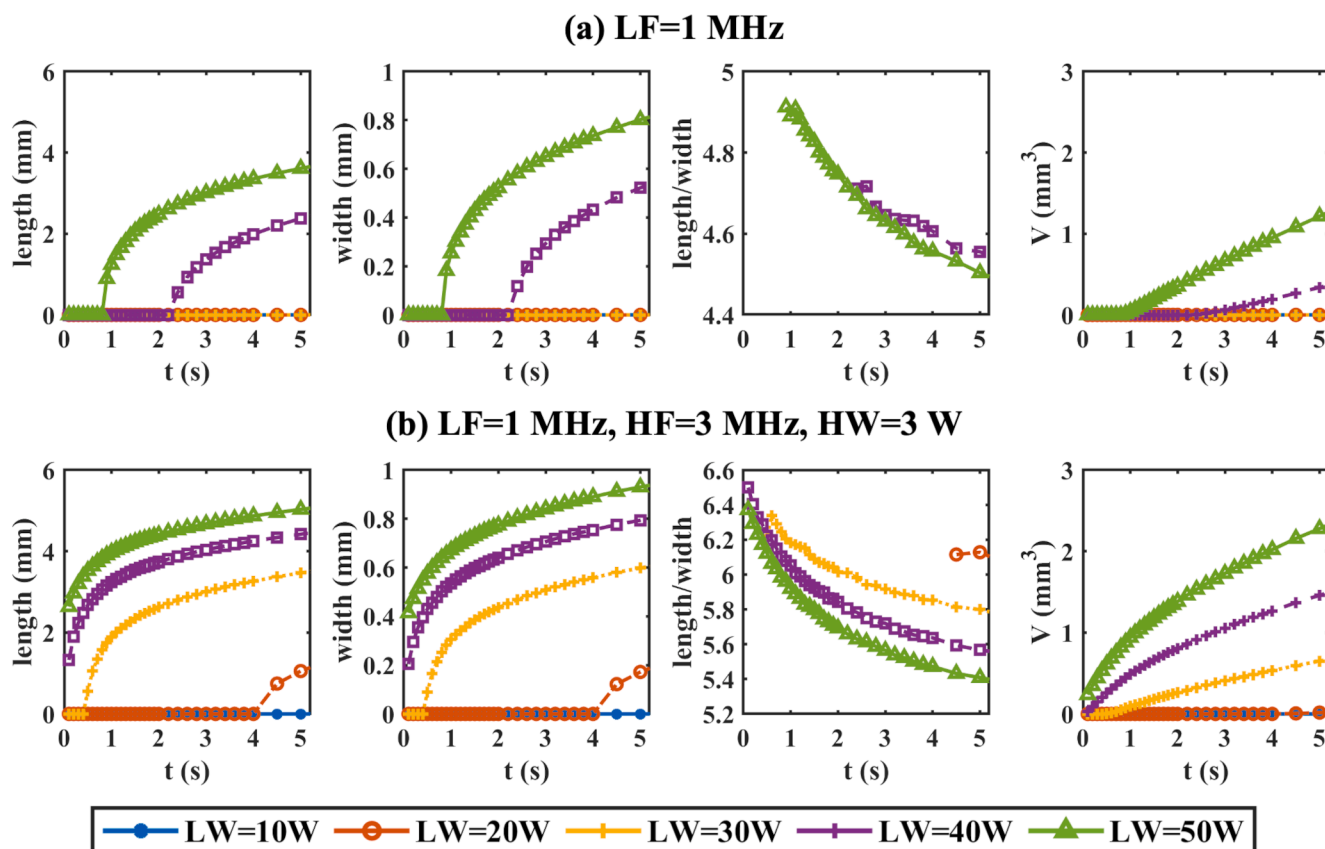


Fig. 8. Dimensions of the nucleation site over time under (a) single- and (b) dual-frequency focused ultrasound conditions. The measures of the nucleation dimensions include the length, width, length–width ratio, and volume of the nucleation region.

effects of different parameters are similar on one measure but complementary on another, e.g. the LF and HF affect the E_j in a same way but have opposite effects on the a/b and V , which makes it possible to control the shape of nucleation region without reducing the nucleation efficiency.

To sum up, in an actual application, the low-frequency ultrasound parameters can be determined first to meet the temperature requirements and allow a coarse adjustment of nucleation volume, then the high-frequency ultrasound parameters will be selected to satisfy the demands on the irradiation duration, nucleation efficiency, and the nucleation region shape. Taking ADV-enhanced HIFU as a specific example, in the treatment regimens combining heat-sensitive drugs or SDT reagents, the temperature of the target area needs to be limited, therefore, a low LW is essential to guarantee a small temperature changes [see Fig. 3] and a moderate LF can be selected to produce a large nucleation area [see Fig. 9]. Then, the HF and HW should be determined to balance the irradiation time, nucleation efficiency, and region shape according to their importance, e.g. a high E_j requirement can select a high HF and optimal HW [see Fig. 5], while a requirement of circle nucleation region can choose a low HF and high HW.

Due to the inclusion of pulsed high-frequency ultrasound, the dual-frequency ultrasound has better flexibility and wider applicability for spatiotemporal control over the nucleation, compared to single-frequency ultrasound. Although the effect of the high-frequency ultrasound depends on the low-frequency ultrasound, the effect can be enhanced through increasing the frequency, acoustic power, and duty cycle of the high-frequency ultrasound. But high duty cycle may enhance the high-frequency thermal effects, which might weaken the independent control over the acoustic pressure and temperature. Therefore, the high-frequency duty cycle is also an important factor that should be investigated in a future research.

3.6. Limitations

The main limitation of this study was that the acoustic field was described using a linear equation and the nonlinear wave propagation was ignored, unlike most focused ultrasound simulations, and especially when using high intensity conditions [44]. However, the dual-frequency ultrasound enables to work at low intensity levels, which reduce nonlinear effects, and thus the linear acoustic behavior assumption holds as mentioned in Section 2.1. Nevertheless, it should be mentioned that nonlinearity amplifies with the increase of driving frequency and acoustic power. Furthermore, the nonlinearity cannot be ignored in the bubble dynamics after the ADV nucleation [53], which will be studied in the future work. In addition, another limitation in this model was the simplification of the Pennes' Bioheat Transfer equation, i.e. Eq. (2), by neglecting the blood perfusion term. Since the maximal irradiation duration was 5 s in the simulation, the blood perfusion could have a visible effect on the temperature and nucleation rate. Therefore, this effect should be considered in the model of human tissue with a large distribution of blood vessels.

4. Conclusions

In this study, ADV nucleation in the dual-frequency focused ultrasound was modeled and the effects of the ultrasound parameters, including driving frequency and acoustic power, on the nucleation rate and efficiency, onset time, and nucleation region volume were investigated. The simulations showed that the addition of a high-frequency pulse enabled to produce a higher nucleation rates, while reducing the required energy. This suggests that the dual-frequency ultrasound has a higher efficacy compared to the single-frequency ultrasound. Furthermore, the high-frequency ultrasound pulse could reduce the nucleation

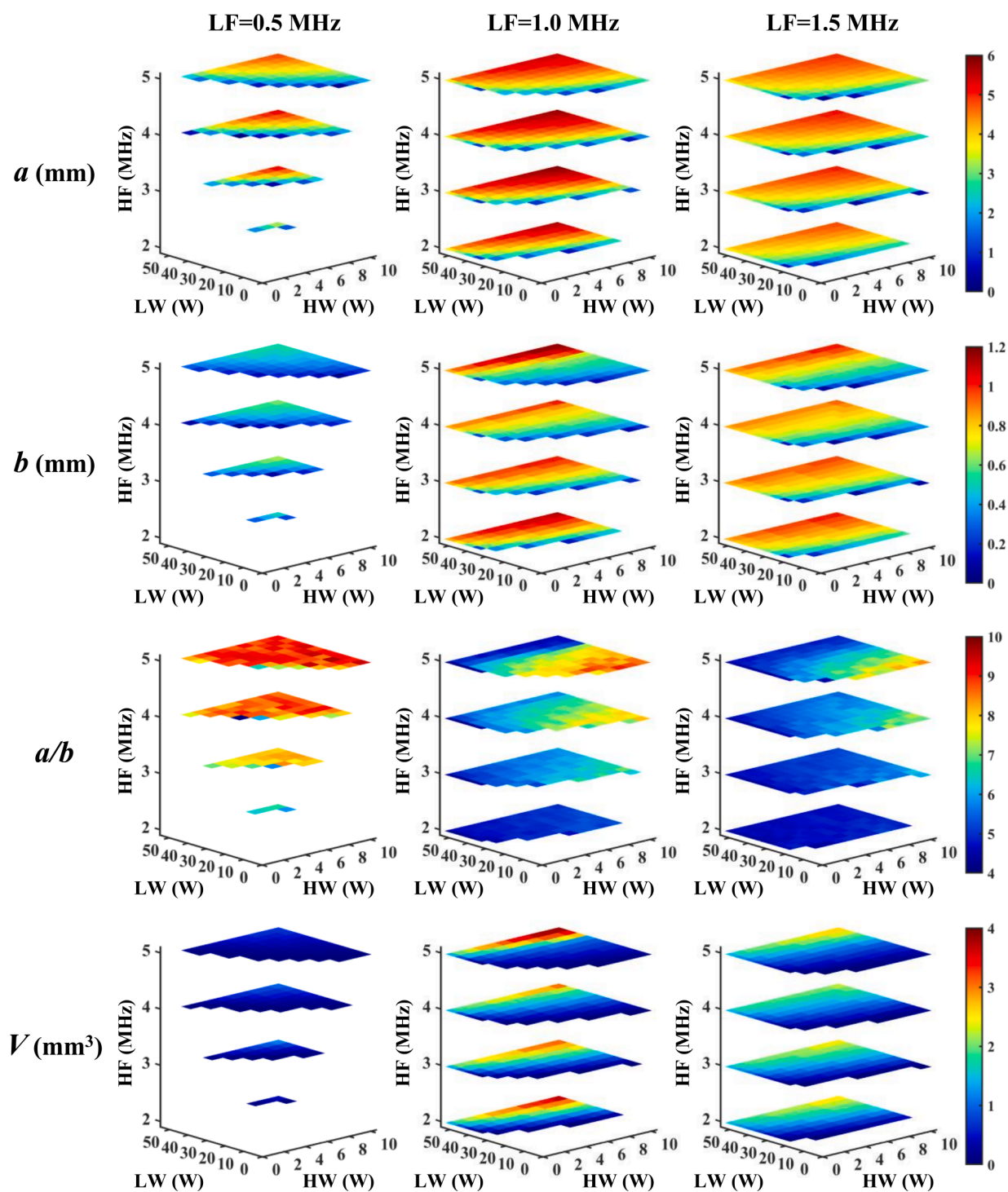


Fig. 9. Dimensions of the nucleation site under different dual-frequency focused ultrasound conditions after 5 s irradiation. The nucleation dimensions include the length a , width b , length–width ratio a/b , and volume V of the nucleation region. Cases with $HW = 0$ are equivalent to the normal single-frequency focused ultrasound conditions. Regions without data indicate conditions of no nucleation.

onset time and increase the length–width ratio of the nucleation region, which enables a fine adjustment of the nucleation site in a spatiotemporal manner. More importantly, the dual-frequency ultrasound realized independent control of both the acoustic and temperature fields, suggesting an optimal regulation of thermal and mechanical effects in ADV nucleation. In summary, the dual-frequency focused ultrasound approach provides an on-demand platform for nucleation regulation, high energy utilization, and reduces complexity that is associated with powerful HIFU systems that operate at a single-frequency. This method

provides a flexible approach that could be compatible in practical applications of on-demand ultrasound theranostics.

Declaration of Competing Interest

The authors declare that they have no known competing financial interests or personal relationships that could have appeared to influence the work reported in this paper.

Data availability

Data will be made available on request.

Acknowledgements

This work was supported by the National Natural Science Foundation of China (Grant No. 82061148015, 11874049, 11904042) and the Israeli Science Foundation (Grant No. 3450/20).

Appendix A. Supplementary data

Supplementary data to this article can be found online at <https://doi.org/10.1016/j.ulsonch.2022.106224>.

References

- [1] G.t. Haar, HIFU tissue ablation: concept and devices, *Ther. Ultrasound* (2016) 3–20.
- [2] R. van Velthoven, F. Aoun, Q. Marcellis, S. Albinini, M. Zanaty, M. Lemort, A. Peltier, K. Limani, A prospective clinical trial of HIFU hemiablation for clinically localized prostate cancer, *Prostate Cancer Prostatic Dis.* 19 (1) (2016) 79–83.
- [3] R.O. Illing, J.E. Kennedy, F. Wu, G.R. ter Haar, A.S. Protheroe, P.J. Friend, F. V. Gleeson, D.W. Cranston, R.R. Phillips, M.R. Middleton, The safety and feasibility of extracorporeal high-intensity focused ultrasound (HIFU) for the treatment of liver and kidney tumours in a Western population, *Br. J. Cancer* 93 (8) (2005) 890–895.
- [4] M.C.L. Peek, F. Wu, High-intensity focused ultrasound in the treatment of breast tumours, *Ecancermedicinescience* 12 (2018) 794.
- [5] D. Coluccia, J. Fandino, L. Schwyzler, R. O’Gorman, L. Remonda, J. Anon, E. Martin, B. Werner, First noninvasive thermal ablation of a brain tumor with MR-guided focused ultrasound, *J. Ther. Ultrasound* 2 (2014) 17–17.
- [6] F. Recker, M. Thudium, H. Strunk, T. Tonguc, S. Dohmen, G. Luechters, B. Bette, S. Welz, B. Salam, K. Wilhelm, E.K. Egger, U. Willner, U. Attenberger, A. Mustea, R. Conrad, M. Marinova, Multidisciplinary management to optimize outcome of ultrasound-guided high-intensity focused ultrasound (HIFU) in patients with uterine fibroids, *Sci. Rep.* 11 (1) (2021) 1–9.
- [7] F. Ziglioli, M. Baciarello, G. Maspero, V. Bellini, T. Bocchialini, D. Cavaliere, E. G. Bignami, U. Maestroni, Oncologic outcome, side effects and comorbidity of high-intensity focused ultrasound (HIFU) for localized prostate cancer. A review, *Ann. Med. Surg.* 56 (2020) 110–115.
- [8] D.L. Miller, N.B. Smith, M.R. Bailey, G.J. Czarnota, K. Hynynen, I.R.S. Makin, et al., Overview of therapeutic ultrasound applications and safety considerations, *J. Ultrasound Med. Am. Inst. Ultrasound Med.* 31 (2012) 623–634.
- [9] V.A. Khokhlova, J.B. Fowlkes, W.W. Roberts, G.R. Schade, Z. Xu, T.D. Khokhlova, T.L. Hall, A.D. Maxwell, Y.-N. Wang, C.A. Cain, Histotripsy methods in mechanical disintegration of tissue: Towards clinical applications, *Int. J. Hyperthermia* 31 (2) (2015) 145–162.
- [10] M.O. de Andrade, S.R. Haqshenas, K.J. Pahk, N. Saffari, Modeling the physics of bubble nucleation in histotripsy, *IEEE Trans. Ultrason. Ferroelectr. Freq. Control* 68 (9) (2021) 2871–2883.
- [11] M.O. de Andrade, S.R. Haqshenas, K.J. Pahk, N. Saffari, The effects of ultrasound pressure and temperature fields in millisecond bubble nucleation, *Ultrason. Sonochem.* 55 (2019) 262–272.
- [12] B. Glickstein, M. Levron, S. Shitrit, R. Aronovich, Y. Feng, T. Iovtsh, Nanodroplet-mediated low-energy mechanical ultrasound surgery, *Ultrason. Sonochem.* 48 (7) (2022) 1229–1239.
- [13] Y.-J. Ho, Y.-C. Chang, C.-K. Yeh, Improving nanoparticle penetration in tumors by vascular disruption with acoustic droplet vaporization, *Theranostics* 6 (3) (2016) 392–403.
- [14] W.G. Pitt, R.N. Singh, K.X. Perez, G.A. Hussein, D.R. Jack, Phase transitions of perfluorocarbon nanoemulsion induced with ultrasound: a mathematical model, *Ultrason. Sonochem.* 21 (2) (2014) 879–891.
- [15] Y. Xin, A. Zhang, L.X. Xu, J.B. Fowlkes, The effects on thermal lesion shape and size from bubble clouds produced by acoustic droplet vaporization, *Biomed. Eng. Online* 17 (2018) 1–14.
- [16] Q. Jin, S.-T. Kang, Y.-C. Chang, H. Zheng, C.-K. Yeh, Inertial cavitation initiated by polytetrafluoroethylene nanoparticles under pulsed ultrasound stimulation, *Ultrason. Sonochem.* 32 (2016) 1–7.
- [17] S.-T. Kang, Y.-C. Lin, C.-K. Yeh, Mechanical bioeffects of acoustic droplet vaporization in vessel-mimicking phantoms, *Ultrason. Sonochem.* 21 (5) (2014) 1866–1874.
- [18] E. Vlasisavljevic, K.-W. Lin, A. Maxwell, M.T. Warner, L. Mancia, R. Singh, A. J. Putnam, B. Fowlkes, E. Johnsen, C. Cain, Z. Xu, Effects of ultrasound frequency and tissue stiffness on the histotripsy intrinsic threshold for cavitation, *Ultrason. Sonochem.* 41 (6) (2015) 1651–1667.
- [19] N. Chang, S. Lu, D. Qin, T. Xu, M. Han, S. Wang, M. Wan, Efficient and controllable thermal ablation induced by short-pulsed HIFU sequence assisted with perfluorohexane nanodroplets, *Ultrason. Sonochem.* 45 (2018) 57–64.
- [20] L.-Q. Zhou, P. Li, X.-W. Cui, C.F. Dietrich, Ultrasound nanotheranostics in fighting cancer: Advances and prospects, *Cancer Lett.* 470 (2020) 204–219.
- [21] S.K. Berlinda Law, Y. Zhou, High-intensity focused ultrasound ablation by the dual-frequency excitation, *IEEE Trans. Ultrason. Ferroelectr. Freq. Control* 66 (1) (2019) 18–25.
- [22] S. Guo, X. Guo, X. Wang, D. Zhou, X. Du, M. Han, Y. Zong, M. Wan, Reduced clot debris size in sonothrombolysis assisted with phase-change nanodroplets, *Ultrason. Sonochem.* 54 (2019) 183–191.
- [23] Y. Li, Y. Liu, R. Li, M. Lu, X. Wang, Y. Geng, Q. Zhang, M. Wan, Histotripsy liquefaction of large hematoma for intracerebral hemorrhage using millisecond-length ultrasound pulse groups combined with fundamental and second harmonic superposition: A preliminary study, *Ultrason. Sonochem.* 46 (5) (2020) 1244–1257.
- [24] D. Suo, B. Govind, J. Gu, P.A. Dayton, Y. Jing, Dynamic assessment of dual-frequency microbubble-mediated sonothrombolysis in vitro, *J. Appl. Phys.* 125 (2019) 084702.
- [25] K. Ninomiya, K. Noda, C. Ogino, S.-I. Kuroda, N. Shimizu, Enhanced OH radical generation by dual-frequency ultrasound with TiO₂ nanoparticles: its application to targeted sonodynamic therapy, *Ultrason. Sonochem.* 21 (1) (2014) 289–294.
- [26] C.J. Miles, C.R. Doering, O.D. Kripfgans, Nucleation pressure threshold in acoustic droplet vaporization, *J. Appl. Phys.* 120 (2016) 034903.
- [27] Y. Zhang, Y. Zhang, Chaotic oscillations of gas bubbles under dual-frequency acoustic excitation, *Ultrason. Sonochem.* 40 (2018) 151–157.
- [28] Z. Li, Q. Zou, D. Qin, Enhancing cavitation dynamics and its mechanical effects with dual-frequency ultrasound, *Phys. Med. Biol.* 67 (2022) 085017.
- [29] D. Suo, B. Govind, S. Zhang, Y. Jing, Numerical investigation of the inertial cavitation threshold under multi-frequency ultrasound, *Ultrason. Sonochem.* 41 (2018) 419–426.
- [30] Y. Zhang, Rectified mass diffusion of gas bubbles in liquids under acoustic field with dual frequencies, *Int. Commun. Heat Mass Transfer* 39 (10) (2012) 1496–1499.
- [31] F. Li, X. Zhang, H. Tian, J. Hu, S. Chen, R. Mo, C. Wang, J. Guo, Interactions of bubbles in acoustic Lichtenberg figure, *Ultrason. Sonochem.* 87 (2022) 106057.
- [32] S. Xu, N. Chang, R. Wang, X. Liu, S. Guo, S. Wang, Y. Zong, M. Wan, Acoustic droplet vaporization and inertial cavitation thresholds and efficiencies of nanodroplets emulsions inside the focused region using a dual-frequency ring focused ultrasound, *Ultrason. Sonochem.* 48 (2018) 532–537.
- [33] J. Chen, Z. Nan, Y. Zhao, L. Zhang, H. Zhu, D. Wu, Y. Zong, M. Lu, T. Ilovitsh, M. Wan, Enhanced hifu theranostics with dual-frequency-ring focused ultrasound and activatable perfluoropentane-loaded polymer nanoparticles, *Micromachines* 12 (2021) 1324.
- [34] S. Park, G. Son, Numerical investigation of acoustic vaporization threshold of microdroplets, *Ultrason. Sonochem.* 71 (2021) 105361.
- [35] M. Aliabouzar, K.N. Kumar, K. Sarkar, Effects of droplet size and perfluorocarbon boiling point on the frequency dependence of acoustic vaporization threshold, *J. Acoust. Soc. Am.* 145 (2019) 1105.
- [36] A.D. Maxwell, C.A. Cain, T.L. Hall, J.B. Fowlkes, Z. Xu, Probability of cavitation for single ultrasound pulses applied to tissues and tissue-mimicking materials, *Ultrason. Sonochem.* 39 (3) (2013) 449–465.
- [37] J. Huang, R.G. Holt, R.O. Cleveland, R.A. Roy, Experimental validation of a tractable numerical model for focused ultrasound heating in flow-through tissue phantoms, *J. Acoust. Soc. Am.* 116 (4) (2004) 2451–2458.
- [38] Y. Atsuhiko, M.T. Suchimoto, T. Honma, An analysis of axisymmetric modified Helmholtz equation by using boundary element method, *IEEE Trans. Magn.* 26 (1990) 1015–1018.
- [39] M.F. Hamilton, D.T. Blackstock, L.A. Ostrovsky, Nonlinear acoustics, *J. Acoust. Soc. Am.* 105 (1999) 578.
- [40] D. Qin, Y.i. Feng, M. Wan, Modeling photoacoustic cavitation nucleation and bubble dynamics with modified classical nucleation theory, *J. Acoust. Soc. Am.* 138 (3) (2015) 1282–1289.
- [41] D. Qin, Q. Zou, S. Lei, W. Wang, Z. Li, Predicting initial nucleation events occurred in a metastable nanodroplet during acoustic droplet vaporization, *Ultrason. Sonochem.* 75 (2021) 105608.
- [42] I. Kusaka, A scaling function of nucleation barrier based on the diffuse interface theory, *J. Chem. Phys.* 119 (3) (2003) 1808–1812.
- [43] A.M.A. Dias, F. Llovel, J.A.P. Coutinho, I.M. Marrucho, L.F. Vega, Thermodynamic characterization of pure perfluoroalkanes, including interfacial and second order derivative properties, using the crossover soft-SAFT EoS, *Fluid Phase Equilib.* 286 (2) (2009) 134–143.
- [44] T.D. Khokhlova, Y.A. Haider, A.D. Maxwell, W. Kreider, M.R. Bailey, V. A. Khokhlova, Dependence of boiling histotripsy treatment efficiency on HIFU frequency and focal pressure levels, *Ultrason. Sonochem.* 43 (9) (2017) 1975–1985.
- [45] K.J. Pahk, Control of the dynamics of a boiling vapour bubble using pressure-modulated high intensity focused ultrasound without the shock scattering effect: A first proof-of-concept study, *Ultrason. Sonochem.* 77 (2021) 105699.
- [46] E. Vlasisavljevic, O. Aydin, Y.Y. Durmaz, K.-W. Lin, B. Fowlkes, Z. Xu, M.E. H. ElSayed, Effects of droplet composition on nanodroplet-mediated histotripsy, *Ultrason. Sonochem.* 42 (4) (2016) 931–946.
- [47] S. Dey, V.K. Rathod, Ultrasound assisted extraction of beta-carotene from *Spirulina platensis*, *Ultrason. Sonochem.* 20 (2013) 271–276.
- [48] K.J. Pahk, P. Gélât, D. Sinden, D.K. Dhar, N. Saffari, Numerical and experimental study of mechanisms involved in boiling histotripsy, *Ultrason. Sonochem.* 43 (12) (2017) 2848–2861.
- [49] P.A. Mounford, M.A. Borden, On the thermodynamics and kinetics of superheated fluorocarbon phase-change agents, *Adv. Colloid Interface Sci.* 237 (2016) 15–27.
- [50] K. Davitt, E. Rolley, F. Caupin, A. Arvengas, S. Balibar, Equation of state of water under negative pressure, *J. Chem. Phys.* 133 (2010), 174507.

- [51] K. Davitt, A. Arvengas, F. Caupin, Water at the cavitation limit: Density of the metastable liquid and size of the critical bubble, *EPL* 90 (2010) 16002.
- [52] F. Caupin, A. Arvengas, K. Davitt, M.E.M. Azouzi, K.I. Shmulovich, C. Ramboz, D.A. Sessoms, A.D. Stroock, Exploring water and other liquids at negative pressure, *J. Phys.: Condens. Matter* 24 (2012) 284110.
- [53] L. Ye, X. Zhu, Y. Liu, Numerical study on dual-frequency ultrasonic enhancing cavitation effect based on bubble dynamic evolution, *Ultrason. Sonochem.* 59 (2019) 104744.
- [54] M. Wang, Y. Lei, Y. Zhou, High-intensity focused ultrasound (HIFU) ablation by the frequency chirps: Enhanced thermal field and cavitation at the focus, *Ultrasonics* 91 (2019) 134–149.